Desalination and Water Treatment
www.deswater.com

doi:10.5004/dwt.2019.24572

165 (2019) 212–221
October

Removal of Cr(VI) from acid mine drainage with clay-biochar composite

Hai Wang, Liya Tan, Baowei Hu, Muqing Qiu, Liping Liang, Linfa Bao, Yuling Zhu, Guohe Chen*, Chengcai Huang*

College of Life Science, Shaoxing University, Zhejiang 312000, China, email: wanghai@usx.edu.cn (H. Wang), 799832811@qq.com (L. Tan), hubw1968@163.com (B. Hu), qiumuqing@126.com (M. Qiu), 342546978@qq.com (L. Liang), 1939777274@qq.com (L. Bao), zhuyuling@usx.edu.cn (Y. Zhu), chenguohe@usx.edu.cn (G.H. Chen), chengcai1963@126.com (C. Huang)

Received 1 February 2019; Accepted 16 June 2019

ABSTRACT

A novel biochar-montmorillonite (B@M) composites was synthesized by heating peanut shell B@M and was used to remove Cr(VI) from acid mine drainage (AMD). Batch characterization confirmed that the biochar surface was covered with montmorillonite successfully. The batch adsorption experiment demonstrated that the maximum adsorption capacity of biochar and B@M was 9.18 and 12.18 mg/g, respectively. The adsorption kinetics and isotherms can be satisfactorily fitted by pseudo-second kinetic model and Langmuir model, respectively. No effect of SO_4^{2-} on Cr(VI) removal implied that B@M can simultaneously remove Cr(VI) from SO_4^{2-} aqueous solutions. XPS analysis showed that adsorption, reduction and precipitation were involved in the removal process due to the presence of Fe(II) in montmorillonite. These findings suggested that the engineered biochar-based composite may be a valuable adsorbent for the removal of Cr(VI) from AMD.

Keywords: Biochar; Clay; Cr(VI); Adsorption; Acid mine drainage

1. Introduction

The discharge of acid mine drainage (AMD) produced from mining (e.g., gold, copper, and nickel) caused severe contamination of water as well as soils [1]. AMD was considered as one of the most serious environmental problems in the world due to the co-existence of high concentration of acid, heavy metals and other toxic chemicals, which leaded to long-term impairment to water body and biosphere [2]. These contaminants were non-degradable and would be accumulated in water bodies and enter into the food chains [3]. Therefore, it was compulsive that heavy metals should be removed under the allowable concentrations before discharge into sub-environments [4].

Chromium (Cr) was one of the most contaminants of AMD [5,6]. Generally, soluble Cr(VI) displays much more toxic compared to Cr(III), which can cause perilous impacts on humans, animals, plants and microorganisms [7,8]. Therefore, it was essential to remove Cr from AMD prior to disposal into water and soil. The various conventional remediation techniques, including precipitation, filtration, reduction and ion exchange, have been used to remove Cr(VI) from wastewater in recent years [9–14]. Among these techniques, adsorption was regarded as the most effective and economical method because of low cost, simple operation and ubiquitous adsorbents [15,16]. It has become a hot research topic to choose an adsorption material with strong adsorption capacity, good adsorption selectivity, good chemical stability and low price.

New materials which absorb heavy metals from water bodies have also been developed, such as the novel-nanomaterials, multifunctional nanocomposites and graphene oxide (GO). Yet they still faced various difficulties and challenges in removing heavy metal. Such as the nanosize of the novel-nanomaterials made it easy to aggregate and the surface properties are unstable and easy to oxidize [17]. And the multifunctional nanocomposites and GO composite have the expensive and complicated fabrications [18–20]. In contrast, biochar not only converts all kinds of waste into valuable waste, but also greatly reduces the stress on environmental pollution [21]. Biochar as a type of pyrogenic

*Corresponding author.

1944-3994 / 1944-3986 © 2019 Desalination Publications. All rights reserved.

carbon was generally obtained from agricultural waste. Biochar can be used as an adsorbent to remove heavy metals from wastewater [22–27]. However, the adsorption ability of biochar was needed to be improved, especially in acidic environment [28–32].

As one of the earliest adsorption material-clay minerals were used to modify primary biochar [33]. Montmorillonite as one of the most common clay minerals has great potential in removal of heavy metals and organic compounds due to special physical and chemical properties [34–37]. Montmorillonite was composed of one octahedral unit inner layer between two tetrahedral outer layers [38]. The layers were negatively charged and balanced with hydrated cations existing in the interlayer spaces. However, montmorillonite tended to expand easily, which limited the actual application in wastewater treatment directly. Therefore, the modification of montmorillonite by adding biochar was economic and feasible method to increased adsorption capacity [39,40].

The objectives of this study were (1) to synthesize B@M composites and characterize with SEM, TEM, FT-IR, XRD and Brunauer-Emmett-Teller (BET) techniques; (2) to investigate the effect of water chemistry (e.g., pH, cation, anion, temperature and concentrations) on Cr(VI) removal by B@M composites at acid conditions by batch techniques; (3) to demonstrate the interaction mechanism of Cr(VI) on B@M composites using XPS analysis.

2. Materials and methods

2.1. Materials

Montmorillonite was achieved from Sinopharm Chemical Reagent Co., Ltd. The specific surface area of montmorillonite was ~30 m^2/g. Other chemicals of analytical grade were purchased from Shanghai Chemical Co., China. Peanut shell was obtained from vegetable market of Shaoxing City.

2.2. Preparation of B@M composites

The biochar was firstly synthesized by heating peanut shell at 250°C for 3 h. Briefly, peanut shell was washed and dried at 60°C overnight. Then peanut shell was milled into powders. Then the powder was filled in ceramic crucibles with fitted lid and were put in a muffle furnace and burned under oxygen-limited conditions at 250°C for 2 h. The obtained biochar was cooled to room temperature, powdered and passed through a 100-mesh screen. Then 30 g biochar powder and 30 g montmorillonite were added to 600 mL deionized water and mixed for 2 h under magnetic stirring. The mixture was centrifuged and dried at 105°C. B@M was obtained by milling to powder and then through a 100-mesh screen.

2.3. Characterization

The surface morphologies of as-prepared samples were observed with SEM-EDS (JEOL, JSM-6360LV, Japan; OXFORD, X-act) and TEM (JEOL, JEM-1011, Japan). The XRD analysis was conducted in a D/Max-IIIA Powder X-ray Diffractometer (Rigaku Corp., Japan) with graphite-monochromatized Cu-Kα radiation with step size of 0.02° at 25 mA and 35 kV over range from 10 to 80°. NOVA 4200e Surface area and Pore size analyzer (Micromeritics, Empyrean, USA) were used to analyze surface area and pore size. FTIR spectra of the samples were recorded on a Nexus 670 FTIR spectrometer (Thermo Nicolet, Madison) in the wave number range of 400–4000 cm^{-1}. XPS spectra were collected on ESCALAB250 X-ray photoelectron spectrometer (Thermo-VG Scientific, UK) at operated powder of 150 W and the analyzer constant pass energy of 30 eV.

2.4. Adsorption experiment

Adsorption experiments of Cr(VI) on B@M were conducted intriplicate with 250 mL conical flasks. The sorption isotherms were investigated at pH = 2 and temperature = 20, 30 and 40°C. The pH dependence of adsorption was studied at initial pH of 1–14 with negligible volumes of 0.1–1.0 mol/L NaOH/HCl. The influences of Ca^{2+}, Mg^{2+}, SO_4^{2-} and HCO_3^- were also carried out at pH = 2. The flacks were reacted under shaking bath at 30°C for 100 min. At the set intervals, 1 mL of solution mixture was filtrated with 0.45 μm filter membrane. The residual Cr(VI) concentration was determined using a UV-visible spectrophotometer at 540 nm wavelength with the 1,5-diphenylcarbazide method. The adsorption capacities were calculated under different environmental conditions to determine their effects on the reaction. The equilibrium adsorbed concentration, q_e ($mg \cdot g^{-1}$), was determined according to the following equation:

$$q_e = \frac{(C_0 - C_e)V}{m} \tag{1}$$

where C_0 and C_e (mg/L) represent the liquid-phase concentrations of Cr(VI) initially and at equilibrium, respectively; q_e (mg/g) was the equilibrium adsorption capacity; V(L) was the volume of the solution; and m (g) was the mass of the adsorbent. The results were reproducible at most 10% error.

3. Results and discussion

3.1. Characterization

The nanostructure and surface morphology of biochar, montmorillonoid and B@M were characterized with SEM. It can be seen that biochar is relatively smooth (Fig. 1a). As shown in Fig. 1b, montmorillonite presented the heterogeneous pores and cavities with rough structure. The rough structure could increase the surface reactive sites, which was also beneficial for Cr(VI) adsorption [41,42]. B@M displayed many small particulate matters with irregular and porous structure (Fig. 1c), which was suitable for the improvement of adsorption capacity. As shown by EDS analysis, carbon and oxygen element were the two main composition of biochar (Fig. 1e), and silicon, oxygen, aluminum, magnesium, calcium and iron are typical elements of montmorillonoid (Fig. 1f). Leaching experiment showed that Fe in montmorillonoid was mainly Fe(II). EDS spectrum of the B@M demonstrated high peaks for

silicon, oxygen, as well as aluminum and magnesium. Calcium and iron were involved in the B@M (Fig. 1g).

As observed with TEM, particle size of montmorillonoid particles appeared to 30–60 nm with flocculent clusters in diffuse edges (Fig. 2a). The morphology of biochar showed the block-shape (Fig. 2b). TEM image of B@M particles confirmed that stabilization of montmorillonoid on biochar, which could prevent the aggression of montmorillonoid particles (Fig. 2c).

N_2 adsorption-desorption isotherms analysis of B@M was carried out. The BET surface area and BJH total pore volume of the biochar were 2.79 m^2/g and 0.0035 cm^3/g. While, the BET surface area and BJH total pore volume of B@M were 6.18 m^2/g and 0.035 cm^3/g, respectively. The adsorption average pore width of the biochar and B@M were 3.94 and 12.76 nm, respectively. After pyrolysis, the specific surface area and average pore size of the composite materials increased significantly. Most of hemicellulose and cellulose, as well as part lignin in biomass are thermally decomposed at the pyrolysis temperature of 250°C [43]. The release of volatile components facilitated the generation of vascular bundles structure in the composite materials, which improved the specific surface area and average pore size [44].

In the FTIR spectrum of biochar (Fig. 2g), the peak of 3420 cm^{-1} was assigned as -O-H stretching vibration. The band at 1770 cm^{-1} was assigned as stretching vibration of -C=O group, implying the formation of carboxylic groups. The peak of 1660 cm^{-1} is related to the presence of -O-H group [45]. The broad band at approximately 1100 cm^{-1} was attributed to the -Si-O stretching vibration. For B@M, the peaks at 3620, 519 and 468 cm^{-1} were assigned as -NH,Fe-O and Si-O-Si, respectively. FTIR analysis confirmed that B@M displayed oxygen functional group, which increase its adsorption ability.

As shown by XRD patterns in Fig. 2e, two diffraction peaks at 2θ = 11 and 24.5° indicated the formation of biochar [46]. For B@M (Fig. 2f), four peaks at 2θ = 5.7, 20.7, 34.9 and 60.8° were identified as *d*(001), *d*(0211), *d*(130) and *d*(060) planes of montmorillonite [47]. A sharp peak at 2θ = 28.8° was assigned to quartz (SiO_2), which is a common impurity in clay.

3.2. Adsorption kinetics

The adsorption kinetics of Cr(VI) on biochar, montmorillonoid, B@M at pH = 1 and 2 was demonstrated in Fig.

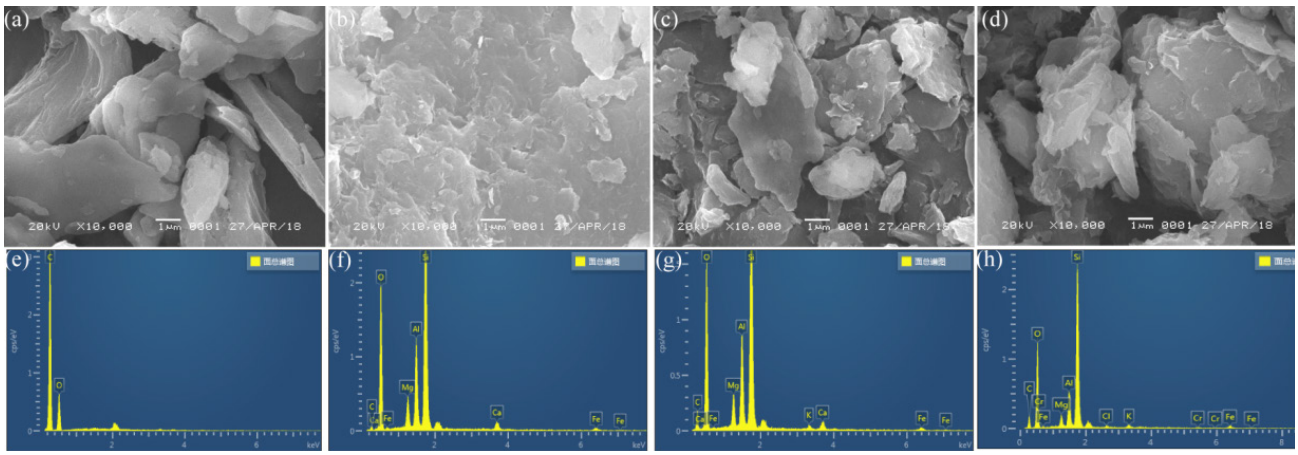

Fig. 1. SEM images and EDS spectra of the biochar (a, e), montmorillonoid (b, f), B@M (c, g) and B@M-Cr (d, h).

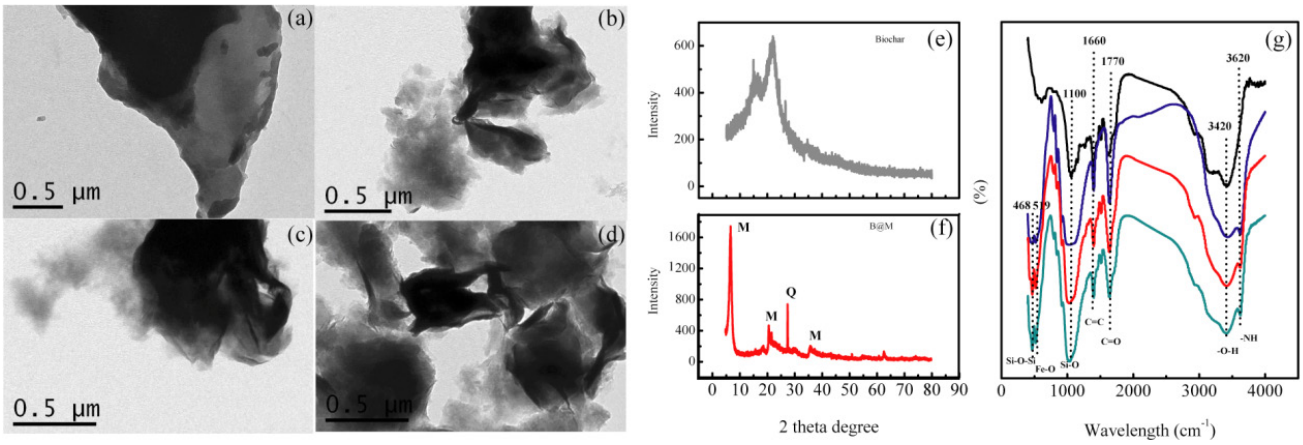

Fig. 2. TEM images of biochar (a), montmorillonoid (b), B@M (c) and B@M-Cr (d). XRD analysis of Biochar (e) and B@M (f). FTIR spectra of Biochar (black), montmorillonoid (blue), B@M (red) and B@M-Cr (green).

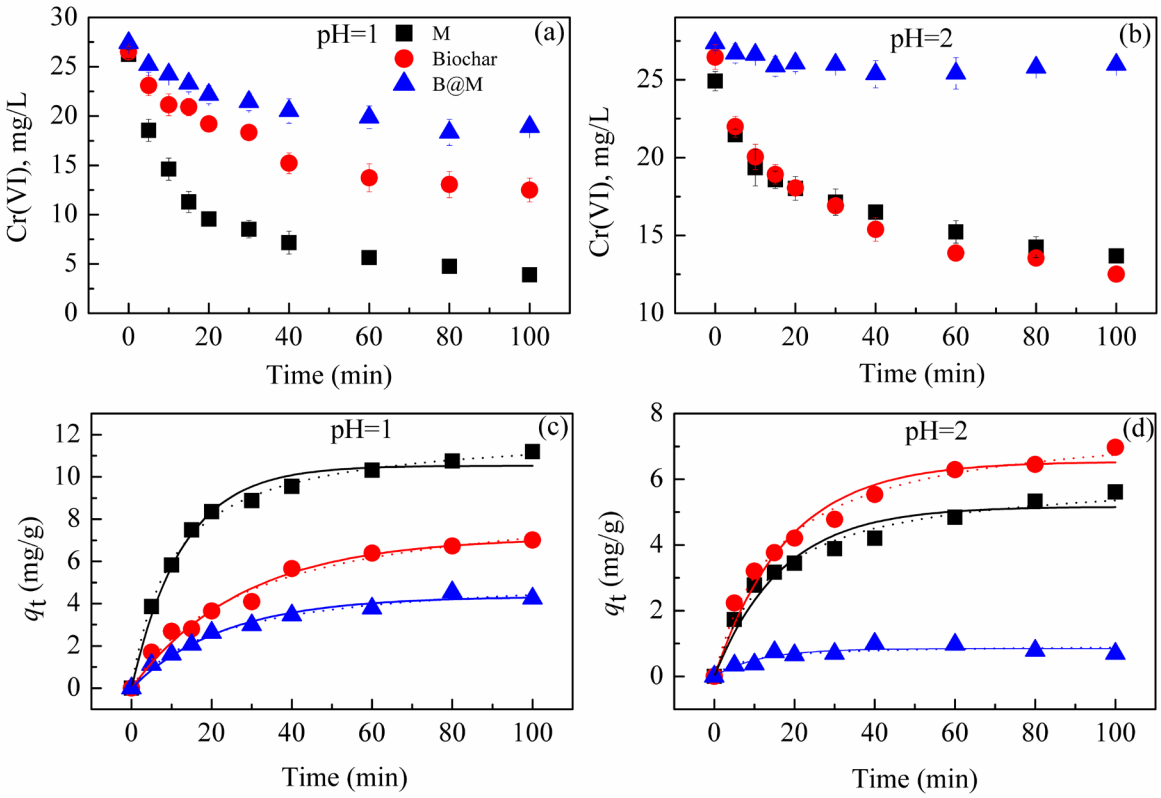

Fig. 3. The effects of B@M, biochar and montmorillonite on the removal of Cr(VI) from the solution at pH = 1 (a) and pH = 2(b). Removal kinetics of B@M, biochar and montmorillonite at pH = 1 and pH = 2. Solid line: fitted by first order kinetics; dotted line: fitted by second order kinetics. C_0 = 25.0 mg/L, m/v = 2 g/L, T = 303 K.

3. At pH = 1, ~ 85.5%, 52.8%, 30.9% of Cr(VI) was removed by B@M, biochar and montmorillonoid, respectively. It was indicated that B@M displayed the high adsorption ability for Cr(VI) in acidic conditions. However, ~45%, 52.7% and 5.0% of Cr(VI) was removed by B@M, biochar and montmorillonoid at pH = 2, respectively.

Although adsorption of Cr(VI) on B@M at pH = 2 was smaller than that of biochar, removal rate of Cr(VI) on B@M was higher than that of biochar and montmorillonoid, which was attributed to synergistic effect in the immobilization process. It was reported that, clay minerals could reduce Cr(VI) to Cr(III) [48]. Fig. 3 showed that immobilization of Cr(VI) by montmorillonoid was insignificant. It was supposed that cluster of clay powder reduce the removal efficiency, which was in accordance with the previous study.

The removal data was fitted with pseudo-first-order and pseudo-second-order models. The linear forms of first-order and pseudo-second-order models can be described as Eqs. (2) and (3), respectively:

$$\ln(q_e - q_t) = \ln q_e - k_1 t \tag{2}$$

$$\frac{t}{q_t} = \frac{1}{k_2 q_e^2} + \frac{t}{q_e} \tag{3}$$

where q_t and q_e (mg/g) were the amount of Cr(VI) adsorbed on solid at time and equilibrium, respectively. k_1 and k_2 were the pseudo-first-order and pseudo-second-order rate constants, respectively.

The fitted parameters of pseudo-first-order and pseudo-second-order models are listed in Table 1. The removal kinetics of Cr(VI) on the three materials were better fitted by pseudo-second-order kinetic model with higher R^2 values compared to pseudo-first-order kinetic model. This suggested the chemical adsorption was the rate limiting step for either adsorption process. A similar phenomenon has been observed in Cr(VI) adsorption by used coir pith [49] and ethylenediamine-modified rice hull [50].

At pH = 1, the q_e values of biochar and B@M calculated from pseudo-second-order kinetic model were 9.18 and 12.18 mg/g, respectively, and kinetic rate constants of biochar and B@M were calculated as 0.0034 and 0.0097 min^{-1}, respectively. These results confirmed B@M particles with the high adsorption capacity for Cr(VI) compared to biochar, which were attributed to the prevention of the cluster of clay by using biochar. In addition, the introducing of various oxygen containing groups increases the adsorption efficiency and removal rate accordingly.

3.3. Effect of pH value

The pH value in an aqueous solution was one of the most important parameters affecting surface charge and ionization of adsorbent and speciation of the adsorbate. Fig. 3a showed the effect of pH on Cr(VI) removal by B@M. The highest removal of Cr(VI) was observed at pH = 1. Approximately 57 and 85% of Cr(VI) were removed from wastewater in 15 and 120 min, respectively. The removal

Table 1
Parameters of pseudo-first-order and pseudo-second-order kinetic model for Cr(VI) ions removal by the composite materials at pH = 1 and pH = 2

		Pseudo-first-order			Pseudo-second-order		
		q_e (mg/g)	k_1 (min^{-1})	R^2	q_e (mg/g)	k_2 (min^{-1})	R^2
pH = 1	B@M	10.53	0.079	0.9852	12.18	0.097	0.9969
	Biochar	7.14	0.036	0.9766	9.18	0.034	0.9808
	montmorillonite	4.34	0.043	0.9819	5.43	0.043	0.9881
pH = 2	B@M	5.17	0.059	0.9526	6.13	0.011	0.9845
	Biochar	6.54	0.056	0.9674	7.80	0.0082	0.9899
	montmorillonite	0.845	0.088	0.8432	0.947	0.1288	0.8060

Table 2
Parameters of pseudo-first-order and pseudo-second-order kinetic model for Cr(VI) ions removal by the composite materials at different pH value

	Pseudo-first-order			Pseudo-second-order		
	q_e (mg/g)	k_1 (min^{-1})	R^2	q_e (mg/g)	k_2 (min^{-1})	R^2
pH = 1	10.53	0.079	0.985	12.18	0.097	0.997
pH = 2	4.78	0.019	0.964	6.34	0.0099	0.992
pH = 3	4.03	0.013	0.937	4.69	0.0066	0.993
pH = 13	2.52	0.019	0.929	3.38	0.018	0.991
pH = 14	2.79	0.027	0.882	6.09	0.033	0.998

rates of Cr(VI) at pH = 2 and 3 were 45.0 and 27.4%, respectively. However, the adsorption of Cr(VI) from the wastewater was negligible at pH = 4–12. It was noted that the removal efficiency at pH = 13 and 14 was increased from 22.6 to 46.38%. The data of removal kinetics were fitted by pseudo-first-order and pseudo-second-order models. The calculated parameters of pseudo-first-order and pseudo-second order kinetic model are shown in Table 2. The removal kinetics of Cr(VI) on biochar, montmorillonoid and B@M were satisfactorily fitted by pseudo-second-order kinetic model according to of the high correlation coefficient ($R^2 > 0.99$), implying that the predominant adsorption of Cr(VI) on biochar, montmorillonoid and B@M were chemisorption process. As illustrated by Cr(VI) distribution in Fig. 4d, the major Cr(VI) specie was $Cr_2O_7^{2-}$ at pH < 6, whereas CrO_4^{2-} was the main specieat pH > 9. Therefore, the high adsorption of Cr(VI) on B@M at low pH could be attributed to electrostatic attraction of negative Cr(VI) and positive charged B@M. At pH = 2, Cr(VI) existed in the solution in forms of $Cr_2O_7^{2-}$ and $HCrO_4^-$, they were attached on the surface on B@M via electrostatic attraction.

Fig. 5 showed FTIR spectra of biochar, montmorillonoid and B@M at different pH conditions. At pH = 7, the typical bands of B@M at 468, 519, 1100, 1660, 1770 and 3420 cm^{-1} were attributed to Si-O-Si, Fe-O, Si-O,-OH group, respectively [51]. However, the new band of B@M at pH 14 at 3130 cm^{-1} was assigned to -C=CH group. The decreased of adsorption intensities of -OH and -NH groups imply interaction of biochar and clay at acid conditions. For example, the presence of -C=CH group was attributed to the interaction of acid/base with biochar.

3.4. Adsorption isotherms

Fig. 6 showed the adsorption isotherms of Cr(VI) under different temperatures. The removal rate of Cr(VI) gradually increased with increasing temperature from 20 to 40°C, indicating favorable adsorption of Cr(VI) at high temperature. The data of adsorption isotherms were fitted by Langmuir and Freundlich models. The linear form of Langmuir and Freundlich equations are written as Eqs. (4) and (5), respectively:

$$\frac{C_e}{Q_e} = \frac{C_e}{Q_{\max}} + \frac{1}{K_L Q_{\max}} \tag{4}$$

$$\log Q_e = \log K_F + \frac{1}{n}\log C_e \tag{5}$$

where C_e (mg/L) and Q_e (mg/g) represent the equilibrium concentration of Cr(VI) at solution and at solid, respectively; Q_{max} was the theoretical maximum adsorption capacity (mg/g); K_L and K_F represent the Langmuir constant (L/mg) and the Freundlich constant [(mg/g) (L/mg)$^{1/n}$], respectively; 1/n was the heterogeneity factor.

The sorption isotherms of Cr(VI) on the composite materials are shown in Figs. 6b and 6c. The relative parameters of Langmuir and Freundlich models are listed in Table 3. The sorption isotherms of Cr(VI) on the composite materials can be satisfactorily fitted by Langmuir model due to the high correlation coefficient (R^2) values compared to Freundlich model, which was consistent with the previous researches [52,53]. Therefore, it can be assumed that adsorption mainly occurs in monolayers with identical sites on the surface of the composite materials.

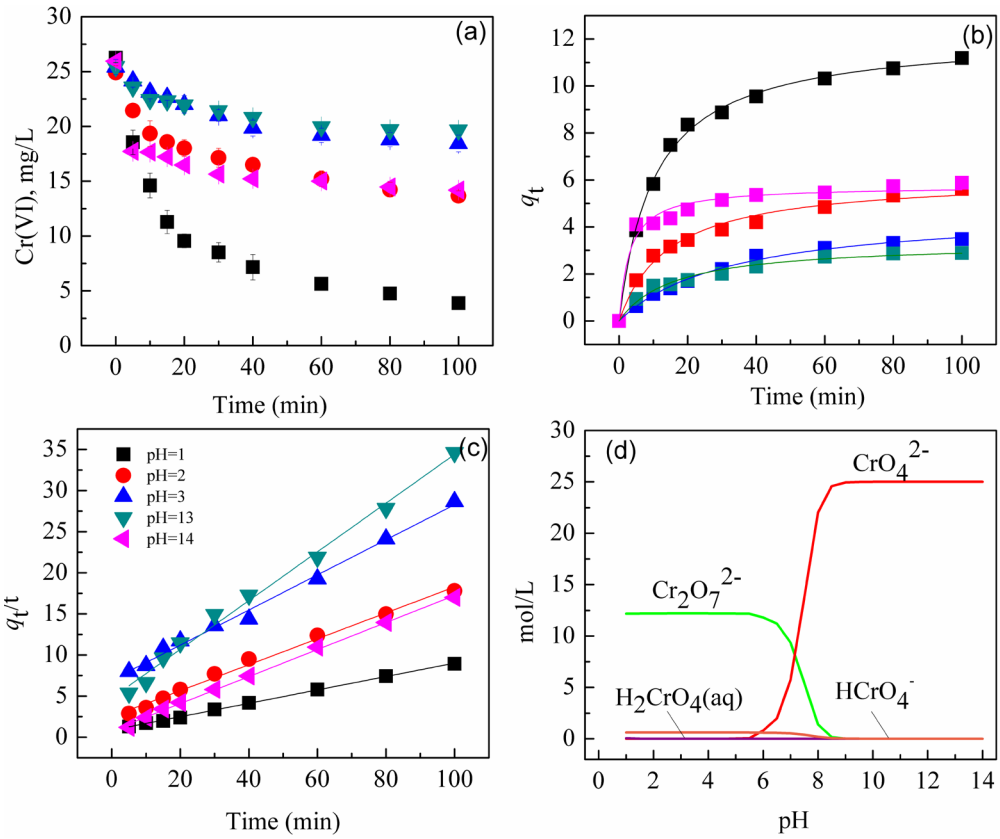

Fig. 4. Effect of pH value in solution on the removal of Cr(VI)ions by the composite materials. C_0 = 25.0 mg/L, m/v = 2 g/L, T = 303 K.

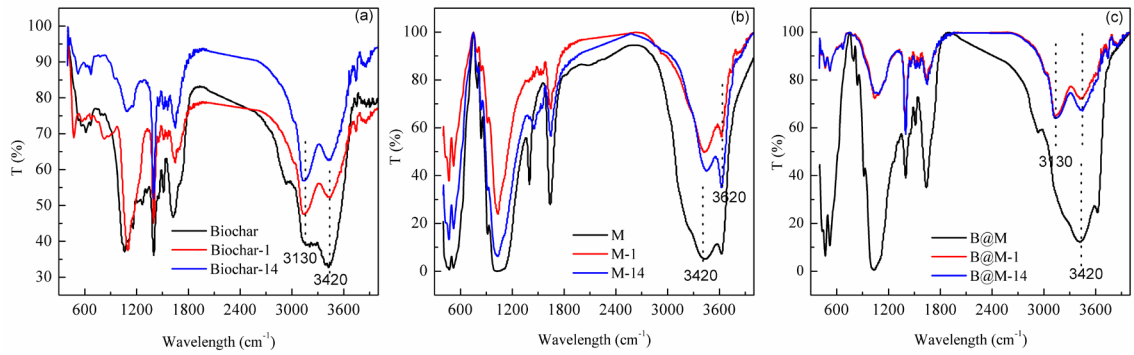

Fig. 5. FTIR spectra of biochar (a), montmorillonite (b) and B@M (c) at different pH.

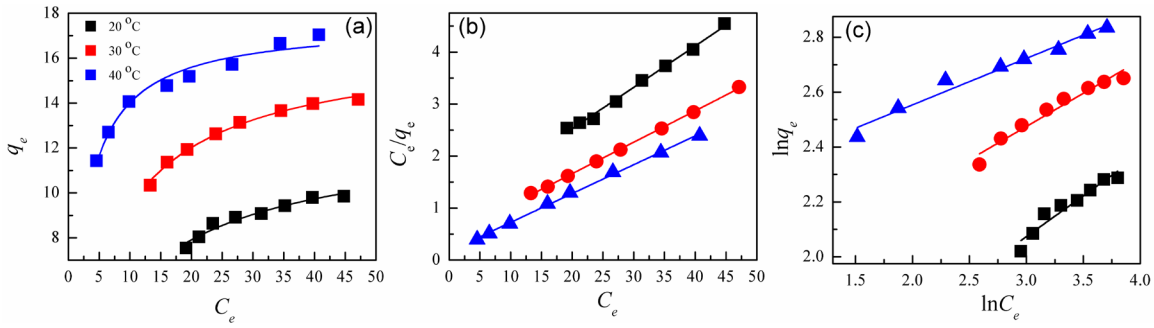

Fig. 6. Effect of temperature in solution on the removal of Cr(VI) ions by the composite materials.

Table 3
Parameters of Langmuir adsorption model and Freundlich adsorption model at different temperature

T	Langmuir adsorption model			Freundlich adsorption model		
	q_m (mg/g)	k_L (L/mg)	R^2	k_F	$1/n$	R^2
20°C	12.56	0.085	0.993	3.25	0.297	0.922
30°C	16.56	0.134	0.999	5.75	0.241	0.949
40°C	18.05	0.327	0.998	9.16	0.169	0.970

Table 4
Parameters of pseudo-first-order and pseudo-second-order kinetic model for Cr(VI) removal by the composite materials in the solution containing Ca^{2+} and Mg^{2+}

Ca^{2+}	q_e (mg/g)	k_2 (min^{-1})	R^2	Mg^{2+}	q_e (mg/g)	k_2 (min^{-1})	R^2
0 mol/L	6.12	0.012	0.985	0 mol/L	6.12	0.012	0.985
0.05 mol/L	5.87	0.010	0.995	0.05 mol/L	6.32	0.0087	0.982
0.1 mol/L	5.66	0.011	0.994	0.1 mol/L	5.42	0.014	0.955
0.15 mol/L	5.63	0.0089	0.986	0.15 mol/L	5.40	0.012	0.929
0.2 mol/L	5.56	0.007	0.969	0.2 mol/L	5.08	0.014	0.977

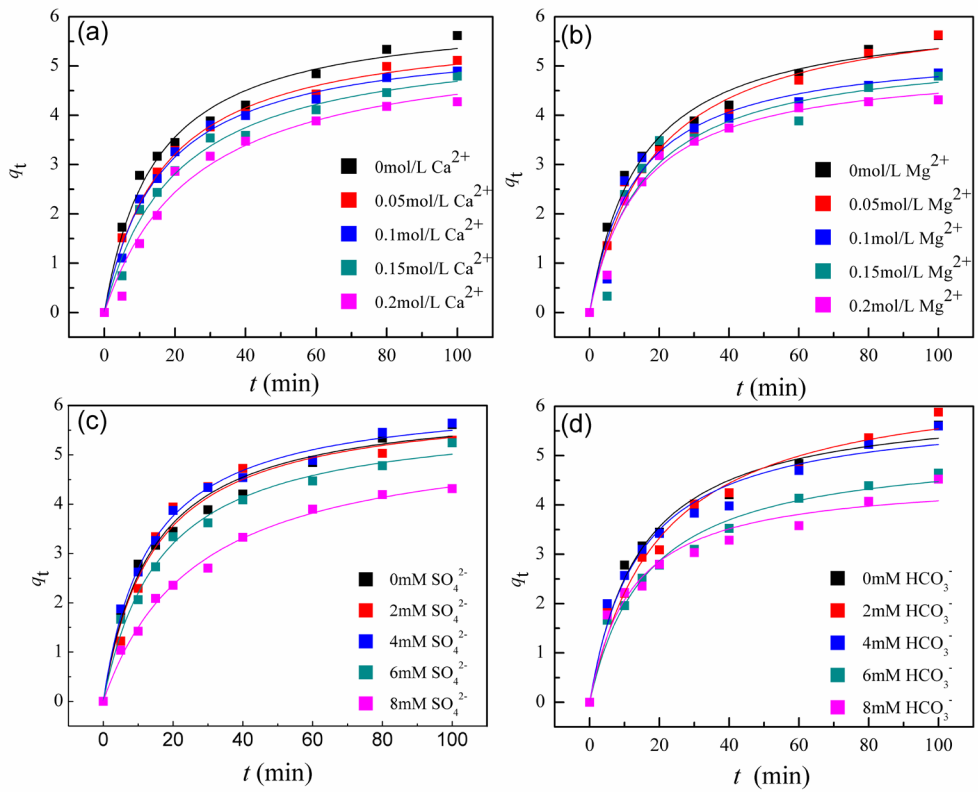

Fig. 7. Effect of Ca^{2+}, Mg^{2+}, SO_4^{2-} and HCO_3^- on the removal of Cr(VI) by the composite materials. C_0 = 25.0 mg/L, m/v = 2 g/L, T = 303 K.

3.5. Effect of various ions

The Fig.7a showed the influence of Ca^{2+} on removal of Cr(VI) by B@M composites. No significant impact of Ca^{2+} on Cr(VI) removal was observed at lower than 0.05 mol/L. At Ca^{2+} > 0.05 mol/L, the removal efficiency decreased from 45.06 to 39.91%, and the rate constant of pseudo-second-order model was also decreased from 0.012 to 0.010 min^{-1}. At concentration of Ca^{2+} = 0.2 mol/L, the rate constant and removal efficiency were 0.007 min^{-1} and 36.58%, respectively.

The effect of Mg^{2+} on Cr(VI) removal is shown in Fig. 7b. Mg^{2+} inhibited the adsorption of B@M. The q_e decreased from 5.42 to 5.08 mg/g with increasing Mg^{2+} from 0.1 to 0.2 mol/L. Previous study indicated that no Ca^{2+}/Mg^{2+} oxide

or hydroxide were formed on the surface of the particles, at low concentration. While, at high concentration, a film was generated on the surface of B@M because of the interaction between Ca^{2+}/Mg^{2+} and the oxygen-containing group in biochar, which prevented the contact of pollutant and active sites.

The effect of SO_4^{2-} on Cr(VI) removal with B@M is shown in Fig. 7c. SO_4^{2-} displayed slight effect on both rate constants and removal efficiency of Cr(VI) at 2 and 4 mM. However, the removal efficiency of Cr(VI) at SO_4^{2-} = 8 mM (38.31%) were significantly lower than that of Cr(VI) removal in the absence of SO_4^{2-} (45.06%). SO_4^{2-} at high concentration was the competitor for $Cr_2O_7^{2-}$ and $HCrO_4^-$, which will occupy the reactive site on the biochar and resulted in the decreased removal rate of Cr(VI).

Fig. 7d illustrates the effect of HCO_3^- on Cr(VI) removal. It was clearly that HCO_3^- decreased the removal efficiency of the composites. Within 100 min, the adsorption capacity significantly increased from 4.58 to 6.12 mg/g with decreased HCO_3^- from 4.0 to 0 mmol/L (Table 5), which was in good accordance with previous researches. It was pointed out that HCO_3^- could connect with the proton in B@M, which resulted in the passivation of active sites and decreased adsorption ability [54]. Another explanation for the inhibitory influence may be that addition of HCO_3^- will increase the pH value of the solution, and the removal rate of Cr(VI) was decreased with the increase of pH value.

3.6. Removal mechanisms

XPS analysis of C1s and Cr 2p is presented in Fig. 8. XPS peak of C1s can be deconvoluted to four sub-peaks at 284.5, 286, 292.5, 295.2 ev, attributing to C-C, C-H, C-O, and -COOH group [55,56]. The peaks of Cr 2p XPS spectra at 576.6 and 586.1 eV were attributed to Cr 2p3/2, and Cr 2p1/2, respectively. The occurrence of peaks of 579.4 and 588.4 eV was assigned to Cr(III), indicating reduction of Cr(VI) to Cr(III) [57,58]. Kwak et al. reported that 1.0 kg montmorillonite can released 25.1 mmol Fe(II), which lead to the reduction of Cr(VI) to Cr(III) [48]. The result of EDS and FTIR also confirmed the presence of Fe involved in B@M. In acidic condition, the interaction mechanisms can be described as follows:

$$2HCrO_4^- + 16H^+ + 3Fe^{2+} \rightarrow 2Cr^{3+} + 3Fe^{3+} + 8H_2O_{(l)} \quad (6)$$

$$2CrO_4^{2-} + 16H^+ + 3Fe^{2+} \rightarrow 2Cr^{3+} + 3Fe^{3+} + 8H_2O_{(l)} \quad (7)$$

The adsorption mechanism of Cr(VI) by B@M at acidic conditions is proposed in Fig. 9.

4. Conclusions

A new and low cost absorbent (B@M) was prepared via immobilizing montmorillonite on the surface of biochar. The batch experiments indicated that B@M composite demonstrated the high removal efficiency to Cr(VI) in acidic condition (pH = 1). The removal kinetics and isotherm of Cr(VI) on B@M can be fitted by the pseudo second order model and Langmuir model, respectively. No effect of SO_4^{2-} on Cr(VI) removal under 4 mM. XPS analysis indicated that Cr(VI) was reduced to Cr(III) and then was precipitated on the surface of B@M due to the Fe(II) in montmorillonit.

Table 5
Parameters of pseudo-first-order and pseudo-second-order kinetic model for Cr(VI) removal by the composite materials in the solution containing SO_4^{2-} and HCO_3^-

SO_4^{2-}	q_e (mg/g)	k_2 (min^{-1})	R^2	HCO_3^-	q_e (mg/g)	k_2 (min^{-1})	R^2
0 mmol/L	6.12	0.012	0.985	0 mmol/L	6.12	0.012	0.985
2 mmol/L	6.13	0.012	0.981	2 mmol/L	6.64	0.0076	0.982
4 mmol/L	6.21	0.013	0.994	4 mmol/L	5.96	0.012	0.971
6 mmol/L	5.84	0.010	0.989	6 mmol/L	5.21	0.012	0.979
8 mmol/L	5.51	0.0067	0.994	8 mmol/L	4.58	0.018	0.954

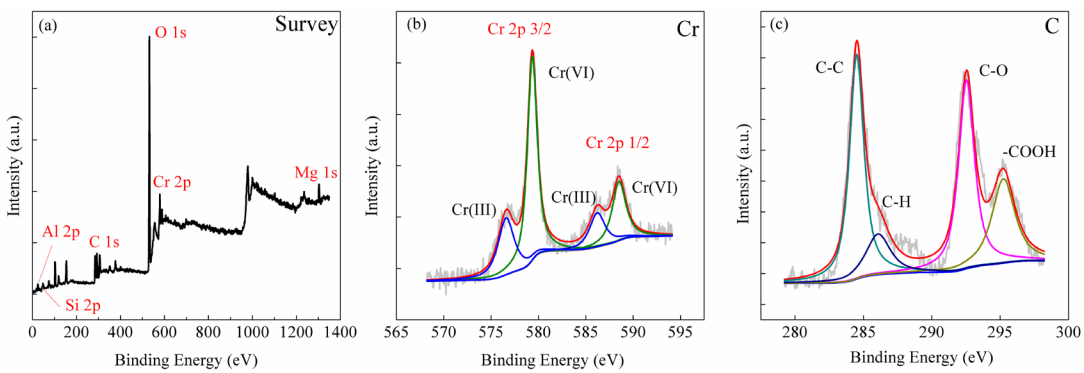

Fig. 8. XPS spectra of survey (a), Cr 2p (b) and C1s (c) high resolution spectra.

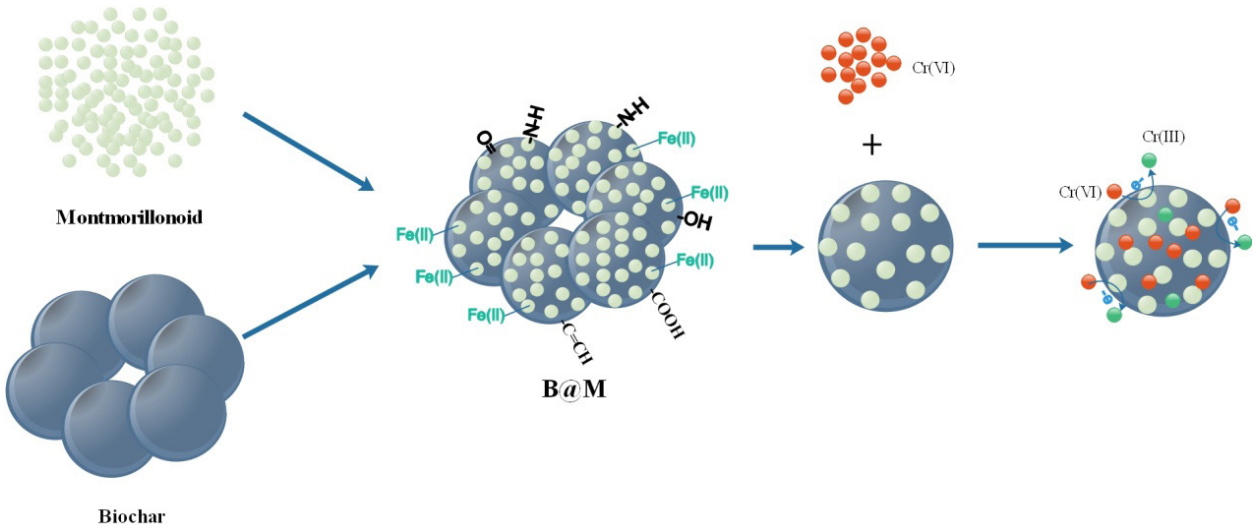

Fig. 9. Preparation process of B@M and the removal mechanism.

These observations indicated that biochar-based composites can be used as the promising adsorbents for the immobilization of heavy metals from AMD.

Acknowledgement

Financial support from the Research Fund Program of National Nature Science Foundation of China (No. 21876115; 41807468; 31500321)

References

[1] A. Azapagic, Developing a framework for sustainable development indicators for the mining and minerals industry, J. Clean. Prod., 6 (2004) 639–662.
[2] A. Akcil, S. Koldas, Acid Mine Drainage (AMD): causes, treatment and case studies, J. Clean. Prod., 14 (2006) 1139–1145.
[3] A. Peppas, K. Komnitsas, I. Halikia, Use of organic covers for acid mine drainage control, Min. Eng., 13 (2000) 563–574.
[4] R. Lauwerys, V. Haufroid, P. Hoet, D. Lison, Toxicologieindustrielle et intoxications professionnelles, 5th ed., Elsevier-Masson, Paris., 2007.
[5] R.A. Gil, S. Cerutti, J.A. Gasquez, R.A. Olsina, Preconcentration and speciation of chromium in drinking water samples by coupling of online sorption on activated carbon to ETAAS determination, Talanta, 68 (2006) 1065–1070.
[6] S. Durairaj, Biosorption of hexavalent chromium in a tannery industry waste water using fungi species, Glob. J. Environ. Sci. Manag., 2 (2016) 105–124.
[7] M. Kobya, Adsorption, kinetic and equilibrium studies of Cr(VI) by hazelnut shell activated carbon, Adsorp. Sci. Technol., 22 (2004) 51–64.
[8] X.Q. Li, J.S. Cao, W.X. Zhang, Stoichiometry of Cr(VI) immobilization using nanoscale zerovalent iron (nZVI): a study with high-resolution X-ray photoelectron spectroscopy (HR-XPS), Ind. Eng. Chem. Res., 47 (2008) 2131–2139.
[9] Q.W. Liang, J.J. Geng, H.J. Luo,W. Fang, Fast and selective removal of Cr(VI) from aqueous solutions by a novel magnetic Cr(VI) ion-imprinted polymerin, J. Mol. Liq., 248 (2017) 767–774.
[10] D. Petruzzelli, R. Passino, G. Tiravanti, Ion exchange process for chromium removal and recovery from tannery wastes, Ind. Eng. Chem. Res., 34 (1995) 2612–2617.
[11] C.A. Kozlowski, W. Walkowiak, Removal of chromium (VI) from aqueous solutions by polymer inclusion membranes, Water Res., 36 (2002) 4870–4876.
[12] F. Akbal, S. Camc, Copper, chromium and nickel removal from metal plating wastewater by electrocoagulation, Desalination, 269 (2011) 214–222.
[13] A. Assadi, M.H. Dehghani, N. Rastkari, S. Nasseri, A.H. Mahvi, Photocatalytic reduction of hexavalent chromium in aqueous solution with zinc oxide nanoparticles and hydrogen peroxide, Environ. Prot. Eng., 38 (2012) 5–16.
[14] T. Mohammadi, A. Moheb, M. Sadrzadeh, A. Razmi, Modeling of metal ion removal from wastewater by electrodialysis, Sep. Purif. Technol., 41 (2005) 73–82.
[15] S.A. Chaudhry, T.A. Khan, I. Ali, Equilibrium, kinetic and thermodynamic studies of Cr(VI) adsorption from aqueous solution onto manganese oxide coated sand grain (MOCSG), J. Mol. Liq., 236 (2017) 320–330.
[16] V.K. Gupta, D. Pathania, S. Sharma, S. Agarwal, P. Singh, Remediation of noxious chromium (VI) utilizing acrylic acid grafted lignocellulosic adsorbent, J. Mol. Liq., 177 (2013) 343–352.
[17] Y.H. Wu, H.W. Pang, Y. Liu, X.X. Wang, Environmental remediation of heavy metal ions by novel-nanomaterials: A review, Environ. Pollut., 246 (2019) 608–620.
[18] Q.L. Fang, J.F. Zhang, L.F. Bai, J.Y. Duan, H.J. Xu, K.C.F. Leung, S.H. Xuan, In situ redox-oxidation polymerization for magnetic core-shell nanostructure with polydopamine-encapsulated-Au hybrid shell, J. Hazard. Mater., 367 (2019) 15–25.
[19] X. Liu, J. Sun, X.T. Xu, A. Alsaedi, T. Hayat, Adsorption and desorption of U(VI) on different-size graphene oxide, Chem. Eng. J., 360 (2019) 941–950.
[20] X. Liu, J. Sun, X.T. Xu, G.D. Sheng, Y.B. Sun, Y.S. Huang, A. Alsaedi, T. Hayat, J.X. Li, Is the interaction between graphene oxide and minerals reversible? Environ. Pollut., 249 (2019) 785–793.
[21] Q. Huang, S. Song, Z. Chen, B.W. Hu, J.R. Chen, X.K. Wang, Biochar-based materials and their applications in removal of organic contaminants from wastewater: state-of-the-art review, Biochar, (2019) https://doi.org/10.1007/s42773-019-00006-5.
[22] J. Lehmann, A handful of carbon, Nature, 447 (2007) 143–144.
[23] C.L. Schelske, Eutrophication: focus on phosphorus, Science, 324 (2009) 722.
[24] D.J. Conley, H.W. Paerl, R.W. Howarth, D.F. Boesch, S.P. Seitzinger, K.E. Havens, C. Lancelot, G.E. Likens, Controlling eutrophication: nitrogen and phosphorus, Science, 323 (2009) 1014–1015.

[25] L. Beesley, E. Moreno-Jimenez, J.L. Gomez-Eyles, E. Harris, B. Robinson, T. Sizmur, A review of biochars' potential role in the remediation, revegetation and restoration of contaminated soils, Environ. Pollut., 159 (2011) 3269–3282.
[26] J. Lehmann, J. Gaunt, M. Rondon, Bio-char sequestration in terrestrial ecosystems – a review, Mitig. Adapt. Strat. GL., (2006) 403–427.
[27] S.P. Sohi, E. Krull, E. Lopez-Capel, R. Bol, A review of biochar and its use and function in soil, Adv. Agron., 105 (2010) 47–82.
[28] M. Zhang, B. Gao, S. Varnoosfaderani, A.F. Hebard, Y. Yao, M. Inyang, Preparation and characterization of a novel magnetic biochar for arsenic removal, Bioresource Technol., 130 (2013) 457–462.
[29] A.U. Rajapaksha, M. Vithanage, M. Zhang, M. Ahmad, D. Mohan, Pyrolysis condition affected sulfamethazine sorption by tea waste biochars, Bioresource Technol., 166 (2014) 303–308.
[30] M. Zhang, B. Gao, Y. Yao, Y.W. Xue, M. Inyang, Synthesis, characterization, and environmental implications of graphene-coated biochar, Sci. Total Environ., 435 (2012) 567–572.
[31] L.B. Qian, W.Y. Zhang, J.C. Yan, L. Han, Y. Chen, D. Ouyang, M.F. Chen, Nanoscale zero-valent iron supported by biochars produced at different temperatures: Synthesis mechanism and effect on Cr(VI), Removal. Environ. Pollut., 223 (2017) 153–160.
[32] M. Zhang, B. Gao, Y. Yao, Y.W. Xue, Synthesis of porous MgO–biochar nanocomposites for removal of phosphate and nitrate from aqueous solutions, Chem. Eng. J., 210 (2012) 26–32.
[33] Y. Xie, C.L. Chen, X.M. Rena, X.X. Wang, H.Y. Wang, X.K. Wang, Emerging natural and tailored materials for uranium-contaminated water treatment and environmental remediation, Prog. Mater. Sci., 103 (2019) 180–234.
[34] D. Ghosh, K.G. Bhattacharyya, Adsorption of methylene blue on kaolinite, Appl. Clay Sci., 20 (2002) 295–300.
[35] A. Kaya, Characterization of clay particle surfaces for contaminant sorption in soil barriers using flow microcalorimetry, J. Environ. Eng., 130 (2004) 918–921.
[36] J. Zhuang, G.R. Yu, Effects of surface coatings on electrochemical properties and contaminant sorption of clay minerals, Chemosphere, 49 (2002) 619–628.
[37] M. Segad, B. Jonsson, T. Akesson, B. Cabane, Ca/Na montmorillonite: structure, forces and swelling properties, Langmuir, 26 (2010) 5782–5790.
[38] A. Gurses, C. Dogar, M. Yalcin, M. Acikyildiz, R. Bayrak, S. Karaca, The adsorption kinetics of the cationic dye, methylene blue, onto clay, J. Hazard. Mater., 131 (2006) 217–228.
[39] H.H. Murray, Overview, clay mineral applications, Appl. Clay Sci., 5 (1991) 379–395.
[40] C. Bilgic, Investigation of the factors affecting organic cation adsorption on some silicate minerals, J. Colloid Interf. Sci., 281 (2005) 33–38.
[41] S. Liu, W.H. Xu, Y.G. Liu, X.F. Tan, G.M. Zeng, X. Li, J. Liang, Z. Zhou, Z.L. Yan, X.X. Cai, Facile synthesis of Cu(II) impregnated biochar with enhanced adsorption activity for the removal of doxycycline hydrochloride from water, Sci. Total Environ., 592 (2017) 546–553.
[42] J.D. Yu, C.Y. Jiang, Q.Q. Guan, P. Ning, J.J. Gu, Q.L. Chen, J.M. Zhang, R.R. Miao, Enhanced removal of Cr(VI) from aqueous solution by supported ZnO nanoparticles on biochar derived from wastewater hyacinth, Chemosphere, 195 (2018) 632–640.
[43] C.N. Hamelinck, G.V. Hooijdonk, A.P.C. Faaij, Ethanol from lignocellulosic biomass: techno-economic performance in short-, middle- and long-term, Biomass Bioenerg., 28 (2005) 384–410.
[44] M. Li, Q. Liu, L.J. Guo, Y.P. Zhang, Z.J. Lou, Y. Wang, G.R. Qian, Cu(II) removal from aqueous solution by Spartina alterniflora derived biochar, Bioresource Technol., 141 (2013) 83–88.
[45] L.B. Qian, W.Y. Zhang, J.C. Yan, L. Han, Y. Chen, D. Ouyang, M.F. Chen, Nanoscale zero-valent iron supported by biochars produced at different temperatures: Synthesis mechanism and effect on Cr(VI) removal, Environ. Pollut., 223 (2017) 153–160.
[46] A. Bogusz, P. Oleszczuk, R. Dobrowolski, Application of laboratory prepared and commercially available biochars to adsorption of cadmium, copper and zinc ions from water, Bioresource Technol., 196 (2015) 540–549.
[47] B.S. Kadu, Y.D. Sathe, A.B. Ingle, R.C. Chikate, K.R. Patil, C.V. Rode, Efficiency and recycling capability of montmorillonite supported Fe-Ni bimetallic nanocomposites towards hexavalent chromium remediation, Appl. Catal. B-Environ., 104 (2011) 407–414.
[48] S.J. Kwak, J.C. Yoo, H. Moon, K. Baek, Role of clay minerals on reduction of Cr(VI), Geoderma, 312 (2018) 1–5.
[49] M. Makehelwala, K.B.S.N. Jinadasa, N. Tanaka, R. Weerasoriya, Adsorption mechanism of Cr(VI) onto coir pith, Bioremediat. J., 13 (2009) 188–197.
[50] P.L. Tang, C.K. Lee, K.S. Low, Z. Zainal, Sorption of Cr(VI) and Cu(II) in aqueous solution by ethylenediamine modified rice hull, Environ. Technol., 24 (2003) 1243–1251.
[51] F. Yang, S.S. Zhang, H.P. Li, S.S. Li, K. Cheng, J.S. Li, D.C.W. Tsang, Corn straw-derived biochar impregnated with α-FeOOH nanorods for highly effective copper removal, Chem. Eng. J., 348 (2018) 191–201.
[52] R. Fu, X. Zhang, Z. Xu, X.P. Guo, D.S. Bi, W. Zhang, Fast and highly efficient removal of chromium (VI) using humus-supported nanoscale zero-valent iron: influencing factors, kinetics and mechanism, Sep. Purif. Technol., 174 (2017) 362–371.
[53] N.H. Kera, M. Bhaumik, K. Pillay, S.S. Ray, A. Maity, Selective removal of toxic Cr(VI) from aqueous solution by adsorption combined with reduction at a magnetic nanocomposite surface, J. Colloid Interf. Sci., 503 (2017) 214–228.
[54] L.B. Qian, W.Y. Zhang, J.C. Yan, L. Han, Y. Chen, D. Ouyang, M.F. Chen, Nanoscale zero-valent iron supported by biochars produced at different temperatures: Synthesis mechanism and effect on Cr(VI) removal, Environ. Pollut., 223 (2017) 153–160.
[55] R.L. Boxman, S. Goldsmith, Mass and surface conductivity gain on polymer surfaces metallized using vacuum arc deposition, Thin Solid Films, 223 (1993) 341–347.
[56] F. Yamamoto, S. Yamakama, Surface grafting of polyethylene by mutual irradiation in methyl acrylate vapor. III. Quantitative surface analysis by x-ray photoelectron spectroscopy, J. Polym. Sci. Polym. Phys., 17 (1979) 1581–1590.
[57] T.P. Moffat, R.M. Latanision, R.R. Ruf, An X-ray photoelectron spectroscopy study of chromium-metalloid alloys-III, Electrochim. Acta., 40 (1995) 1723–1734.
[58] E. Desimoni, C. Malitesta, P.G. Zambonin, J.C. Rivière, An x-ray photoelectron spectroscopic study of some chromium-oxygen systems, Surf. Interface Anal., 13 (1988) 173–179.